STM JOURNALS

Journal of
Polymer & Composites

ISSN: 2321-2810 (Online)
ISSN: 2321-8525 (Print)
Volume 11, Special Issue 13, 2023
DOI (Journal): 10.37591/JoPC

http://engineeringjournals.stmjournals.in/index.php/JoPC/index

Research JoPC

Revealing the Hemodynamic Orchestra: Contrasting Analysis of Blood Flow Patterns in a Bifurcated Carotid Artery

Abdulrajak Buradi[1,*], Sanjaytharan Tamilselvan[2], MD Yousuf Ahmed Khan[3], Kapilan N.[4]

Abstract

Understanding blood flow patterns in the carotid artery (CA) is crucial for detecting cardiovascular diseases. Computational fluid dynamics simulations compared non-Newtonian (non-Newt) and Newtonian (Newt) models under pulsatile and laminar flow. CA geometry was accurately designed using ANSYS Space Claim & Fusion360, and simulations were run in ANSYS Fluent. Discrepancies between non-Newt and Newt models were found, especially in bifurcation's distal regions prone to plaque. Pressure ranged from 27.870 Pa to -107.643 Pa, showing mechanical force variations. Maximum velocity was 0.700 m/s, and some areas experienced stagnant flows. Wall shear stress (WSS) analysis revealed up to 5 Pa, indicating mechanical stress areas. This study underscores blood rheology's role in CA hemodynamics. Comparison between non-Newt and Newt models highlighted significant differences in flow, pressure, and WSS patterns, especially where atherosclerotic plaques develop. These insights are crucial for cardiovascular disease understanding, guiding interventions, and advancing cardiovascular medicine, ultimately enhancing patient care.

Keywords: Carotid artery, Computational fluid dynamics, Newtonian, Non-Newtonian models, Wall Shear Stress

INTRODUCTION

In recent years, the field of biomedical engineering has become increasingly important in advancing healthcare technologies. With the integration of mechanical engineering principles, biomedical engineers have been able to apply fluid dynamics concepts to better understand the flow of blood and other bodily fluids through the human body [1, 2]. This has enabled researchers to better comprehend the development of diseases like atherosclerosis. The carotid artery (CA) plays a substantial part in the cardiovascular system as it supplies oxygenated blood to the brain [3, 4]. It's situated in either side of our neck as seen in Figure 1.

***Author for Correspondence**
Abdulrajak Buradi

[1]Associate Professor, Department of Mechanical Engineering, Nitte Meenakshi Institute of Technology, Govindapura, Bengaluru, Karnataka India
[2]UG Scholar, Department of Mechanical Engineering, Nitte Meenakshi Institute of Technology, Govindapura, Bengaluru, Karnataka India
[3]UG Scholar, Department of Mechanical Engineering, Nitte Meenakshi Institute of Technology, Govindapura, Bengaluru, Karnataka India
[4]Professor, Department of Mechanical Engineering, Nitte Meenakshi Institute of Technology, Govindapura, Bengaluru, Karnataka India

Received Date: October 30, 2023
Accepted Date: November 20, 2023
Published Date: March 26, 2024

Citation: Abdulrajak Buradi, Sanjaytharan Tamilselvan, MD Yousuf Ahmed Khan, Kapilan N. Revealing the Hemodynamic Orchestra: Contrasting Analysis of Blood Flow Patterns in a Bifurcated Carotid Artery. Journal of Polymer & Composites. 2023; 11(Special Issue 13): S229–S247.

Stroke is considered to be one of the leading causes of deaths. Specifically, "CA atherosclerosis" accounts for approximately half of all strokes. This condition is characterized by the presence of plaque ulcerations, which cause a linear reduction in the diameter of the artery's lumen and disrupt local hemodynamics.

The prevalence of the disease tends to be higher in areas of arteries characterized by elevated curvature, intricate geometry, and bifurcation,

where deviations from the typical fluid shear stress and fluid mechanical properties observed in healthy vessels occur. The CA is particularly susceptible to this disease [6].

Lack of sufficient blood supply to the brain can lead to a stroke as depicted in Figure 2. The onset of atherosclerosis typically initiates in the carotid bulb and progresses towards the proximal internal CA. The development of atherosclerosis is intricately related with multiple risk parameters mainly hypertension, smoking, diabetes, and more [7, 8].

Understanding the behavior of hemodynamics in the CA is crucial for unraveling the mechanisms underlying cardiovascular diseases, such as atherosclerosis and stroke. Computational fluid dynamics (CFD) simulations have developed as a robust and influential tool in recent times for studying blood flow dynamics and providing insights into the hemodynamics of the CA. In this study, we aim to compare the behavior of blood flow in the CA by means of non-Newt and Newt models under laminar and pulsatile flow conditions. By examining the differences between these models, we can gain a comprehensive understanding of the impact of blood rheology on CA hemodynamics.

The formulation of accurate computational models is essential for capturing the complex nature of blood flow in the CA. This requires precise geometry representation and mesh generation techniques to ensure reliability and accuracy of the simulations [10]. ANSYS Space Claim and Fusion360 software have been utilized to design geometry, incorporating anatomical details and bifurcation characteristics. The subsequent methodology section will provide a detailed description of the steps taken to formulate the computational models and perform the simulations [11].

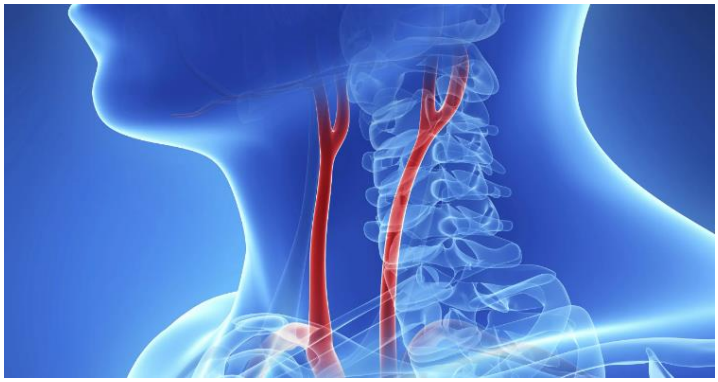

Figure 1. Carotid Artery [5].

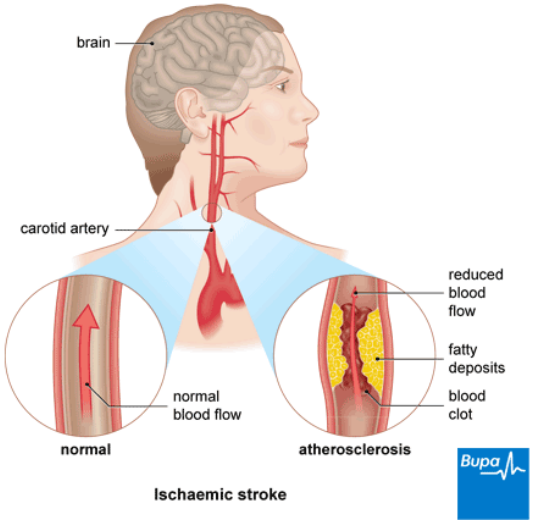

Figure 2. Healthy CA VS Blocked CA [9].

By conducting comparative analysis between non-Newt and Newt models, this study aims to elucidate the role of blood rheology in CA hemodynamics. We expect to observe significant differences in flow behavior, pressure distribution, and wall shear stress (WSS) patterns between these models, particularly in regions prone to atherosclerotic plaque formation. The findings from this study have the potential to provide valuable insights into the pathophysiology of cardiovascular diseases and may guide targeted interventions and advancements in cardiovascular medicine, ultimately leading to improved patient care outcomes.

In the subsequent sections, we will present the formulation, methodology, results, and conclusions of this study. By examining the differences in blood flow dynamics between Newt and non-Newt models, we aim to enhance our understanding of CA hemodynamics and contribute to the growing body of knowledge in the field of cardiovascular research.

FORMULATIONS

To accurately simulate blood flow in the CA, we employed CFD techniques and formulated two models: the non-Newt and Newt model. The Newt model assumes blood to be a homogeneous, isotropic, and Newt fluid, whereas the non-Newt model considers the rheologic blood properties, considering its non-Newt behavior [12,13]. The governing equations for both models are derived from the fundamental Navier-Stokes equations, which effectively define the preservation of momentum and mass in the flow of fluids. In the Newt model, the calculations are constructed on the assumption of constant viscosity, while the non-Newt model incorporates a constitutive equation to capture the shear-thinning behavior exhibited by blood [14].

To represent the complex geometry of the CA, we utilized ANSYS Space Claim and Catia V5 software. These tools allowed us to accurately design the geometry, considering the anatomical details and bifurcation characteristics [15]. We ensured high-quality mesh generation using advanced techniques to capture the intricate features of the geometry. The simulations were conducted using ANSYS Fluent, a widely used software package for CFD analysis. We implemented a time-stepping approach to capture the pulsatile nature of blood flow. Time step sizes of 1.15 seconds and 1.30 seconds were selected to adequately resolve the temporal variations in flow dynamics. The choice of time step size was based on a careful balance between computational efficiency and accuracy [16].

In the subsequent methodology section, we will provide a detailed description of the computational setup, boundary conditions, and mathematical methods employed to unravel the main equations for both Non-newt and Newt models. We will also outline the post-processing methods used to analyze the results and extract relevant hemodynamic parameters [17]. By formulating these models and accurately representing the geometry, we aim to simulate realistic blood flow conditions and investigate the impact of blood rheology on CA hemodynamics. This comprehensive approach will provide valuable insights into the behavior of blood flow in regions prone to atherosclerotic plaque formation, facilitating a better understanding of the underlying mechanisms and potential targets for therapeutic interventions.

METHODOLOGY

The methodology employed in this study aimed to accurately simulate blood flow dynamics in the CA using CFD techniques. The steps involved in formulating the computational models, setting up the simulations, and analyzing the results are described in detail below.

Carotid Artery Geometry

The geometry was designed using ANSYS 2022 R2 Space Claim and Fusion 360 software. Anatomical details, including the vessel diameter, length, were incorporated to ensure realistic representation as seen in Figure 3. The CAD software allowed for precise control over the geometry, ensuring accurate representation of the CA's anatomy and dimensions.

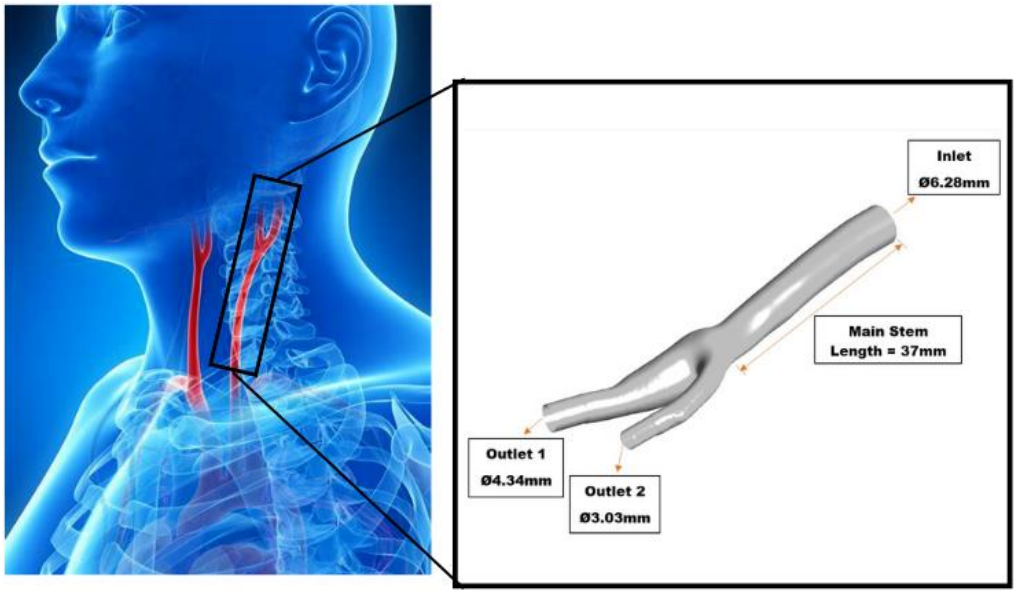

Figure 3. CA model with Dimensions

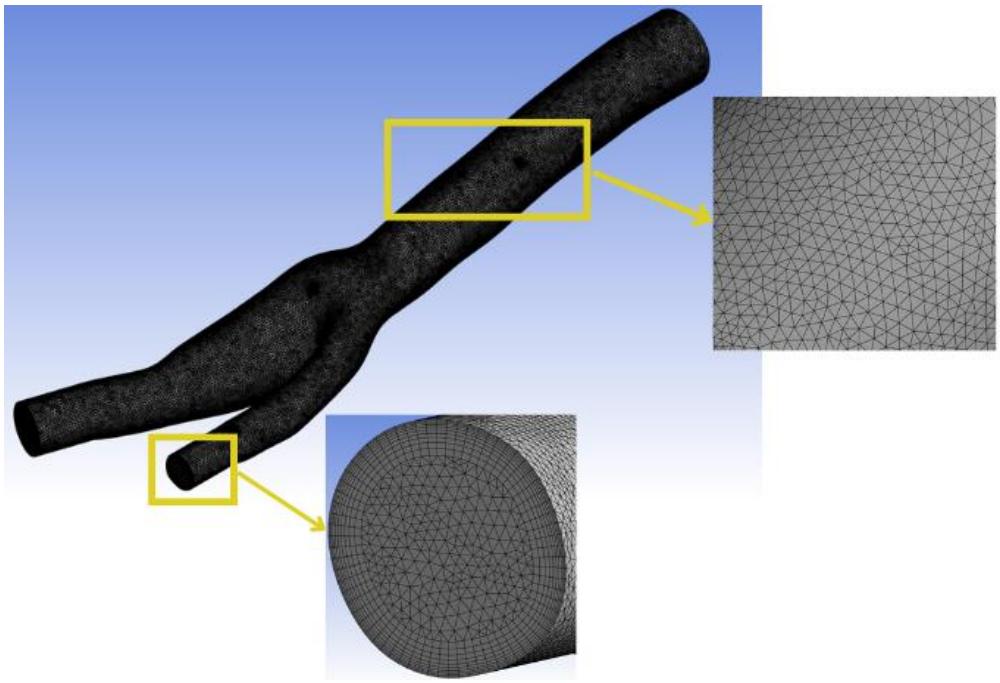

Figure 4. Mesh representation of artery Model.

Mesh Generation and Mesh Independence Study

High-quality mesh generation was crucial to accurately capture the complex features of the CA geometry [18,19]. It was performed using ANSYS 2022 R2 Meshing Application. Based on the complexity of the geometry and the resolution requirements, unstructured mesh was generated which can be observed in Figure 4. Advanced meshing techniques, such as boundary layer meshing, tetrahedral meshing was employed to ensure sufficient mesh resolution near the arterial walls [20, 21]. To ensure a smooth transition, the blood vessel walls are comprised of ten inflation layers, exhibiting a 0.272 ratio of transition. The addition of these layers is necessary for present analysis, as it allows us to closely examine the wall shear [22]. The mesh comprises approximately 645753 elements. The mesh was carefully designed to ensure adequate resolution of the boundary layer near the arterial walls, where significant flow gradients occur.

Furthermore, a mesh independence study was executed to understand the mesh firmness. Multiple meshes with varying levels of refinement were created, and simulations were performed on each mesh. The key hemodynamic parameters of interest, such as pressure distribution and velocity profiles & WSS were compared among the different mesh configurations. The mesh configuration that provided consistent results with minimal variation was selected as the optimal mesh for subsequent simulations. The coarse, medium and fine mesh contained the number of elements 464650, 645753, and 755725 respectively. The detailed mesh independence study is observed in Table 1.

The Figure 5 represents the maximum velocity observed in the velocity profile for different numbers of elements. The x-axis represents the quantity of elements, while the y-axis denotes the maximum velocity. From the graph, we can observe that as the number of elements increases, the maximum velocity tends to increase.

This increase in maximum velocity with a higher number of elements indicates that a finer discretization of the model provides a further detailed depiction of the velocity. As we increase the number of elements, the model is divided into smaller segments, capturing the variations in velocity more precisely. This enhanced resolution helps to capture localized features or fluctuations in the velocity profile, resulting in higher maximum velocity values.

Upon reviewing the Figure 6, it appears that the maximum pressure tends to increase as the number of elements increases. This suggests that a higher resolution or finer discretization of the model, achieved by adding more elements, leads to an increase in the calculated maximum pressure. The increase in maximum pressure with a higher number of elements could be attributed to a more accurate representation of the fluid flow behavior and pressure distribution within the model. With a finer mesh or increased element density, the simulation or measurement can capture smaller-scale variations and intricate details of the flow field. Consequently, this finer resolution can lead to higher pressure estimates at localized regions or near flow obstructions.

Table 1. Mesh Independence Analysis.

Mesh Type	Number of Elements	Max. Velocity (m/s)	Max. Pressure (Pa)	Max. WSS (Pa)
Coarse	464650	1.79094	405.332	69.5036
Medium	645753	1.81201	417.845	81.7405
Fine	755725	1.81387	420.654	82.8556

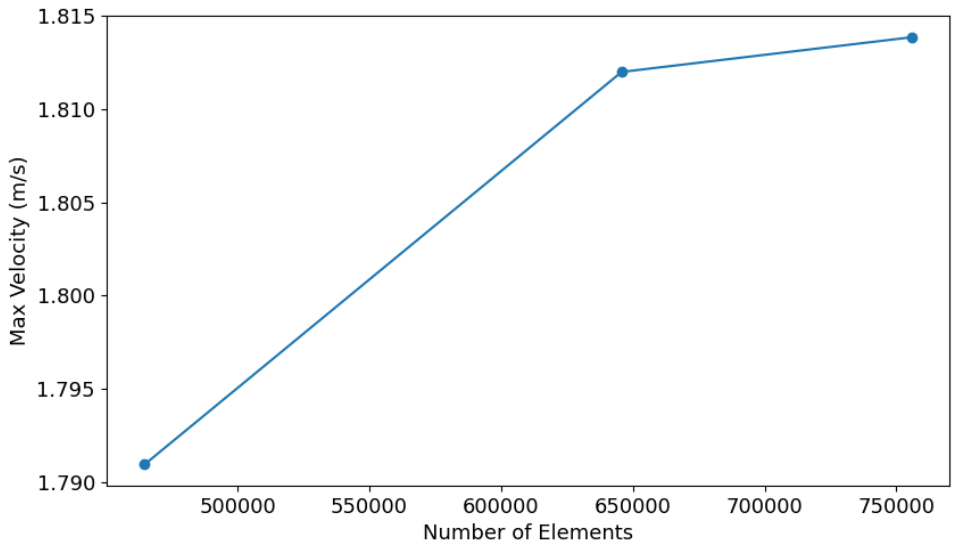

Figure 5. Max Velocity VS Number of Elements.

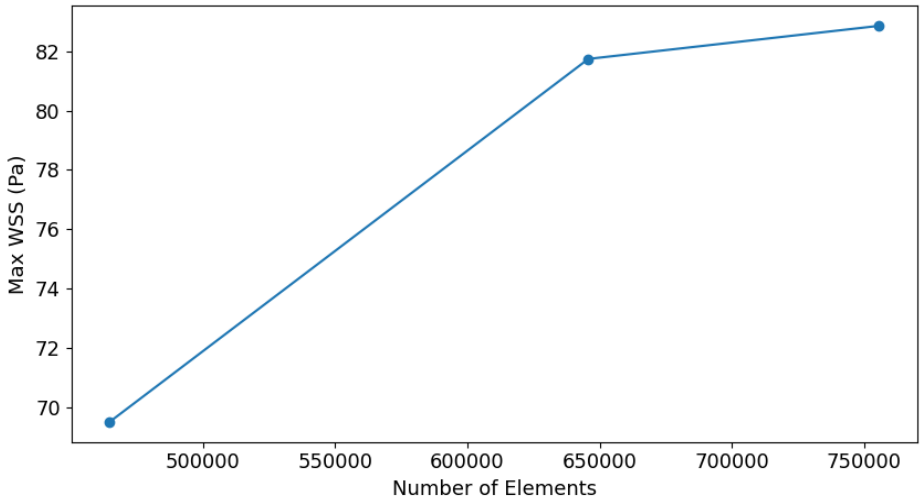

Figure 6. Max Pressure VS Number of Elements.

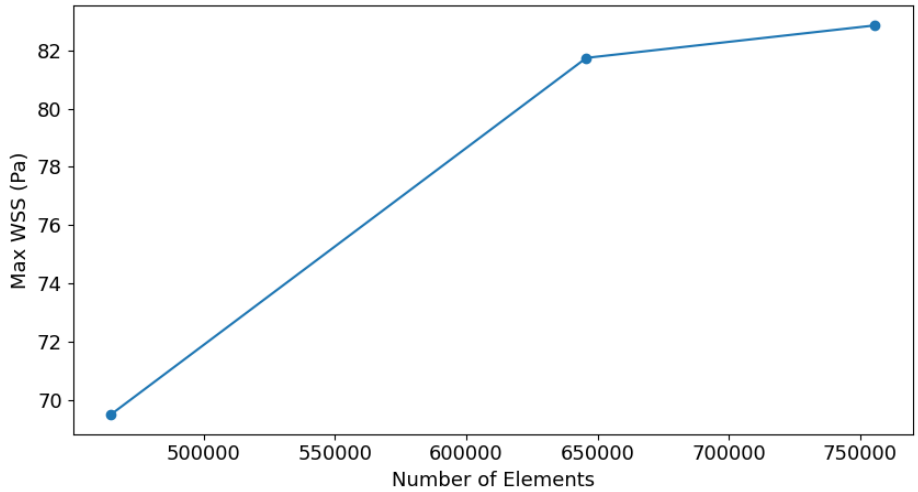

Figure 7. Max WSS VS Number of Elements.

When analyzing the graph of Maximum WSS versus the number of elements (Figure 7), it indicates that the maximum WSS tends to increase as the quantity of elements in the mesh increases [23]. This trend can be attributed to several factors. Firstly, a finer mesh with more elements allows for better resolution of small-scale flow features and variations. As a result, localized regions with higher WSS that were previously undetected by coarser meshes become visible [24]. Consequently, the maximum WSS value increases as the mesh becomes more refined. Furthermore, the intricate artery geometry and flow field nature can contribute to this phenomenon.

Our Mesh Independent Study ensured that the simulations were not excessively computationally demanding while still capturing the essential flow characteristics in the CA accurately. For our research we have chosen Medium Mesh, the chosen optimal mesh balanced the need for computational efficiency with the necessity of resolving the flow features of interest.

Governing Equations and Numerical Methods

The finite volume technique was used to unravel the key flow equations, which govern the flow of fluids. In the case of the Newt model, the momentum and mass conservation equations were used, assuming a constant viscosity. On the other hand, the non-newt model incorporated a constitutive equation, such as the Carreau model, to accurately represent the shear-thinning behavior of blood [23]. The discretized equations were iteratively solved using the commercial solver, ANSYS Fluent.

The continuity equation [21] used in the study is given as:

$$\nabla \cdot (\rho\mu)=0 \quad (1)$$

Where, ρ is the blood density, ∇ · represents the divergence operator, and μ is the velocity vector.

The momentum equations describe the conservation of momentum and account for the pressure gradient, turbulent forces, and any external forces acting on the fluid [21].

In Cartesian coordinates, the momentum equations can be written as:

$$\partial (\rho\mu) / \partial t + \nabla \cdot (\rho\mu \otimes \mu) = -\nabla\rho + \nabla\cdot \tau + f \quad (2)$$

Where, $\partial ((\rho\mu))/\partial t$ represents the rate of change of momentum with respect to time, $\nabla\cdot (\rho\mu \otimes \mu)$ represents the convective term, $-\nabla\rho$ represents the pressure gradient, $\nabla\cdot\tau$ represents the divergence of the viscous stress tensor, f represents any external body forces acting on the fluid.

The viscous stress tensor τ can be expressed as:

$$\tau = \mu(\nabla\mu + \nabla\mu^{\tau}) \quad (3)$$

The Carreau model is another commonly used constitutive equation to describe the non-Newt behavior of fluids, including blood [22]. The Carreau model incorporates shear-thinning effects and is expressed as:

$$\mu = \mu_{\infty} + (\mu_o - \mu_{\infty}) [1 + \lambda\gamma^2]^{\frac{n-1}{2}} \quad (4)$$

Carreau model parameters are mentioned in the Table 2 in detail, additionally a graph between viscosity and strain rate was plotted.

In the Carreau model, as the velocity gradient increases, the viscosity of the fluid decreases from zero shear viscosity (μ_0) to the asymptotic viscosity (μ_∞). The relaxation time (λ) controls the transition from high shear rates to low shear rates. The Carreau model provides a mathematical presentation of the shear-thinning behavior exhibited by many non-newt fluids, including blood. The Relationship between Viscosity & Shear Rate can be seen in Figure 8. It is widely used in CFD simulations to capture the rheological properties of blood more accurately.

Boundary Condition

Physiologically relevant boundary conditions were applied to mimic realistic blood flow conditions. For the inlet conditions, a blood density of 1060 Kg⁄m3 was set and used the Carreau model. A user-defined function (UDF) was incorporated to define the velocity at the inlet. The walls were assigned no-slip conditions, while outlet 1 and outlet 2 were set to outflow conditions.

Pulsatile flow conditions were emulated to capture the dynamic nature of blood flow in the CA. Figure 9 displays the inflow velocity circumstances for 3 cardiac cycles, where each pulsating series has a duration of 0.75 seconds. Time step sizes of 1.15 seconds and 1.30 seconds were chosen based on a balance between computational efficiency and temporal resolution. Hence Contours of 2nd Cardiac Cycle was considered for our study.

Table 2. Carreau model input parameters

Coefficients	Input values
Density (Kg/m^3)	1060
Time Constant, lambda (s)	3.313
Power law index (n)	0.3568
Zero Shear Viscosity (μ_o)	0.056
Infinite Shear Viscosity (μ_∞)	0.00345

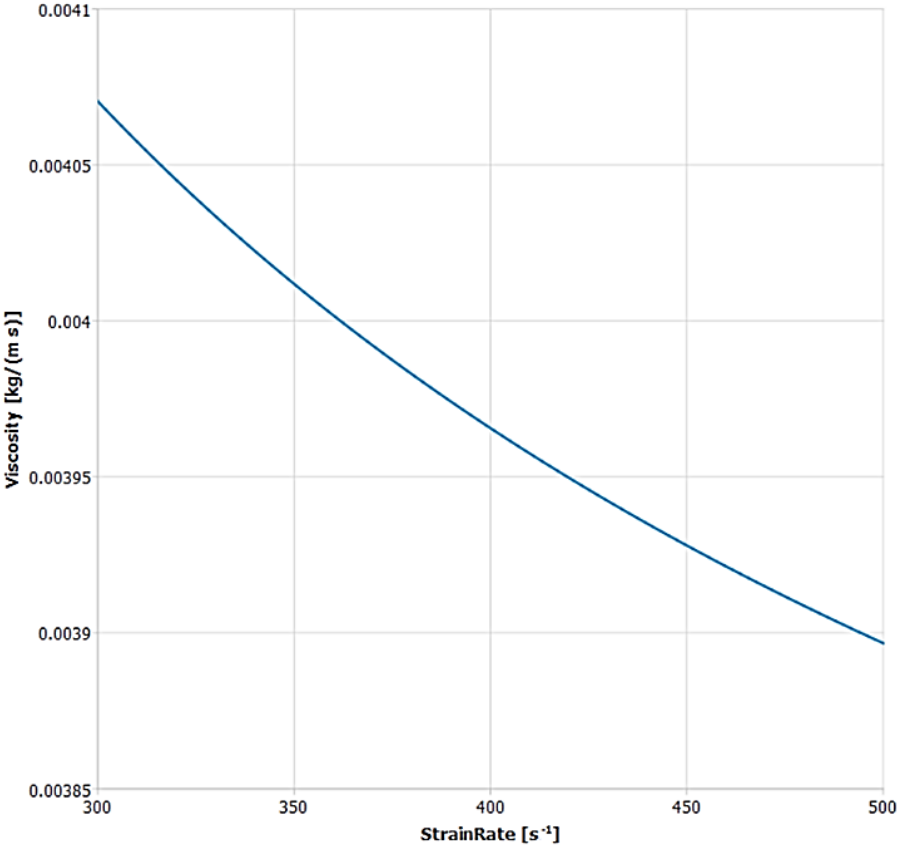

Figure 8. Relation between Viscosity & Strain Rate.

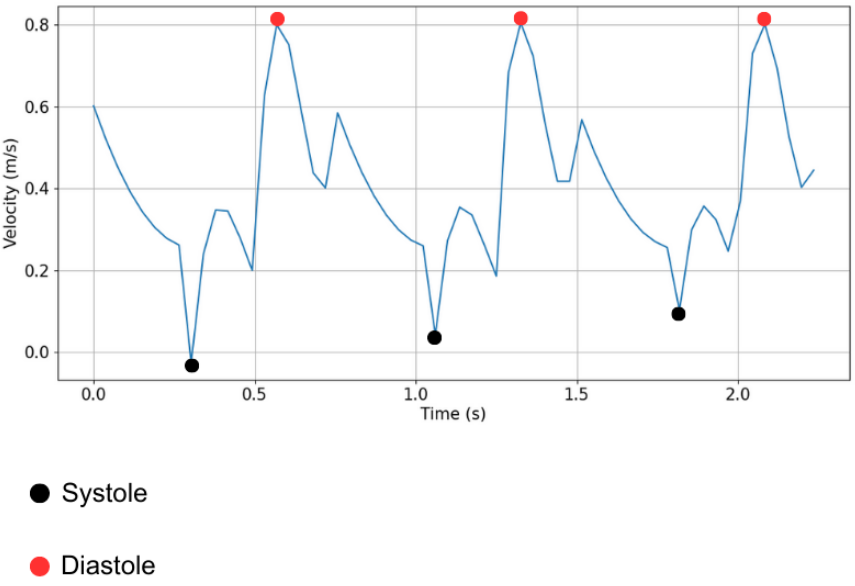

Figure 9. Velocity profile of the blood given at inlet.

Post-Processing & Analysis

The simulation results were post-processed using visualization and analysis tools available in ANSYS CFD Post 2022 R2. Quantities of interest, such as pressure distribution, velocity profiles, and WSS, were extracted and analyzed. Specific attention was given to regions prone to atherosclerotic plaque formation, such as the distal regions of the bifurcation. Visualizations, such as contour plots and streamlines, were generated to provide a firm understanding of the flow patterns and their variations.

In the subsequent Results section, we will present and discuss the findings obtained from the simulations, focusing on the alterations between the Non-newt and Newt models. These results will shed light on the hemodynamic behavior in the CA and its significance in the development of cardiovascular diseases.

Flow Behavior

The velocity distributions obtained from the simulations reveal significant differences between the Non-newt and Newt models. In regions of the CA susceptible to atherosclerotic plaque formation, distinct flow outlines emerge. Stagnant or recirculating flows are observed in these regions, indicating potential areas of disturbed flow associated with a higher risk of plaque deposition. Additionally, the flow velocity profiles exhibit variations between the two models. The addition of the non-newt model accounts for the shear-thinning behavior of blood, leading to modified flow velocities and flow patterns in comparison to the Newt model.

Figure 10 illustrates the velocity distribution of the Newt model at a time step of 1.15 seconds. The regions with low velocity are depicted, indicating areas where the velocity is relatively low. This low velocity is attributed to the low WSS present in those regions, which will be discussed in more detail later. The low velocity leads to significant flow recirculation, which is also depicted in the figure. In Figure 11, the velocity streamlines at a time step of 1.30 seconds for the same Newt model are depicted. It can be observed that Figure 10 and Figure 11 exhibit a striking similarity, highlighting the presence of vicious recirculation of flow in the region with low velocity.

Figure 12 presents the velocity distribution for the non-newt model at two different time steps. Upon comparison with its Newt counterpart, it is evident that the regions of low velocity are similar. However, in the Non-newt model, there is an absence of severe flow recirculation. The depicted figure illustrates that the flow performance in the non-newt model deviates from that of the Newt model, with less pronounced recirculation patterns observed.

The absence of severe flow recirculation in Figure 12 can be attributed to the shear-thinning behavior of blood. The Non-newt viscosity model, Carreau model, accounts for such behavior and decreases the effective viscosity of the blood as the shear rate increases [25]. Flow recirculation typically occurs in regions where there are flow separation and low velocity, often accompanied by the formation of vortices [26]. In the Newt model, the viscosity remains constant which results in the formation of noticeable recirculation patterns in regions characterized by low velocity.

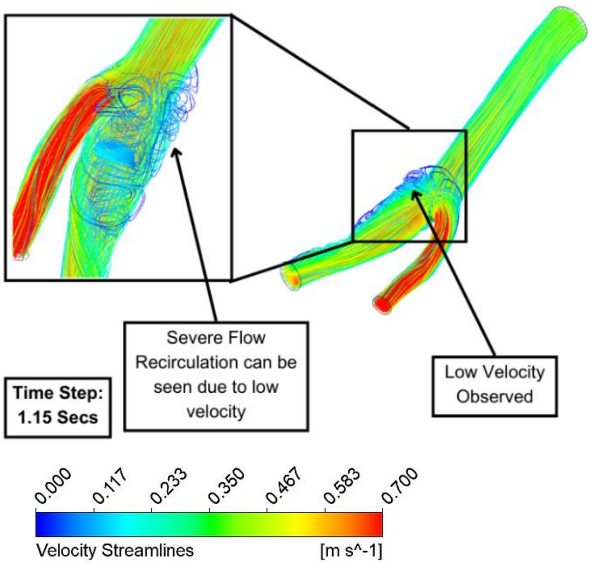

Figure 10. Velocity streamlines of Newtonian Model at 1.15 Secs.

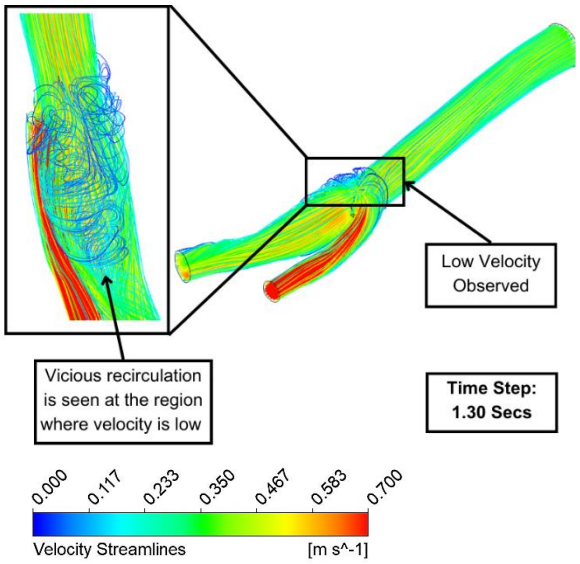

Figure 11. Velocity distribution of Newtonian Model at 1.30 Secs.

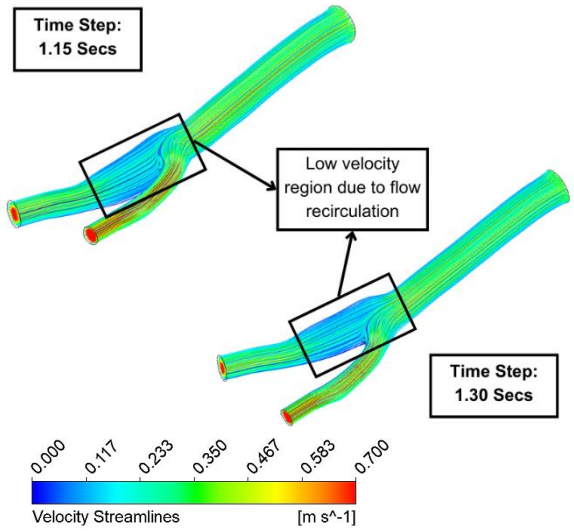

Figure 12. Velocity streamlines for non-Newtonian model.

However, in the Non-newt model, the shear-thinning behavior of blood results in a decrease in viscosity as the shear rate increases. This reduction in viscosity allows the blood to flow more easily and reduces the formation of vortices and recirculation zones [25]. Consequently, due to the shear-thinning behavior of blood, the non-newt model demonstrates reduced flow recirculation in comparison to the Newt model. The presence of shear-thinning behavior in the non-newt model promotes a smoother flow pattern with a reduced tendency for flow separation and recirculation. This behavior is consistent with the observed velocity distribution in Figure 12, where the flow in the non-newt model shows a more streamlined and less recirculating nature compared to the Newt model. It is vital to see that the absence of severe flow recirculation in the non-newt model does not imply the complete elimination of recirculation. Some degree of recirculation may still be present, but it is generally less pronounced due to the effect of the shear-thinning viscosity behavior.

Figure 13 displays a side-by-side comparison of the velocity distributions in the CA for both the Non-newt and Newt models. The contour represents the magnitude of the velocity, ranging from blue (minimum velocity) to red (maximum velocity). The corresponding legend indicates that the observed velocity values range from 0 m/s to a maximum of 0.7 m/s. we can observe contrast differences between

the Non-newt and Newt models in terms of their velocity distributions. The comparison depicted in Figure 13 provides valuable intuitions into the impact of blood rheology on the flow dynamics in the CA. It showcases the influence of the non-newt viscosity model on the flow characteristics, particularly in terms of reducing flow recirculation. These findings significantly enhance our comprehension of the intricate hemodynamic phenomena transpiring in the CA and their potential implications in the onset and progression of cardiovascular diseases.

In conclusion, the analysis of Figures 10, 11, 12, and 13 sheds light on the intricate hemodynamic behavior within the CA under different modeling approaches. The findings emphasizes the critical role of blood rheology in shaping the hemodynamics of the CA and highlight the importance of incorporating non-newt viscosity models to capture more realistic flow behavior.

Pressure Distribution

The pressure profiles obtained from the simulations demonstrate variations amid the Non-newt and Newt models. In Figure 14, the pressure contours of the Newt model at time steps of 1.15 seconds and 1.30 seconds are presented. Upon visual examination, it can be observed that there is minimal difference between the pressure distributions at these two time steps. This observation can be attributed to the characteristics of the CA geometry, which contribute to a relatively steady flow pattern. Due to the specific geometric features of the CA, including the size, shape, and curvature of the vessel, the flow experiences a relatively stable and continuous pattern [23].

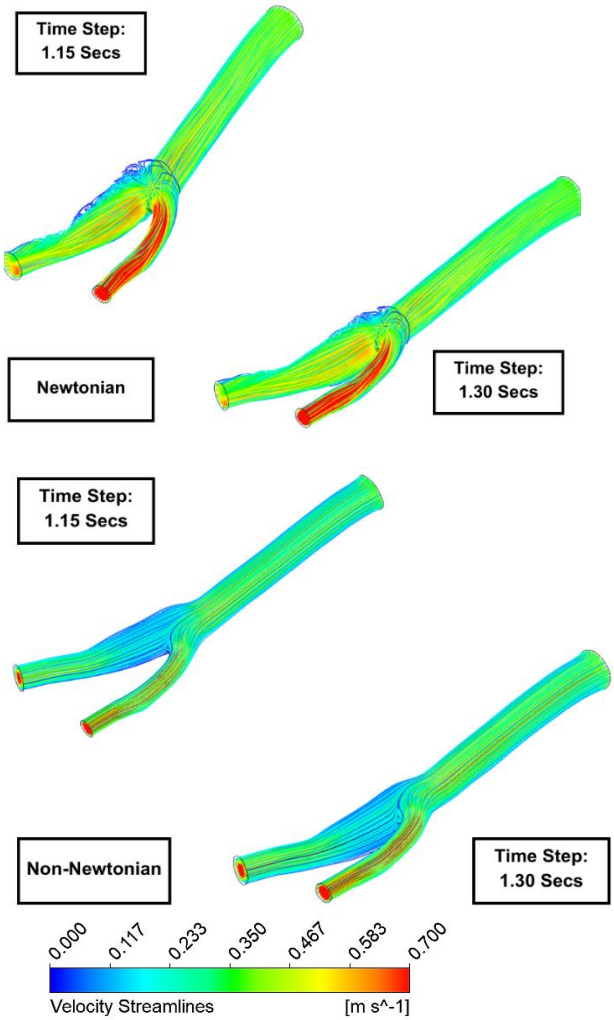

Figure 13. Comparative Visuals of both Non-Newtonian and Newtonian models.

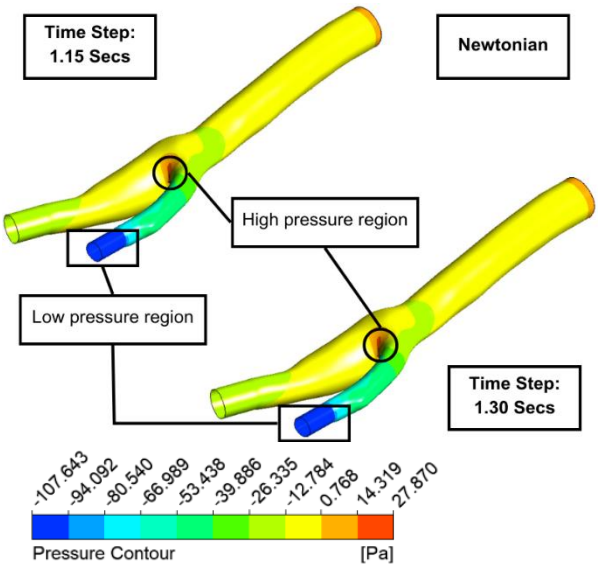

Figure 14. Pressure contours of Newtonian model.

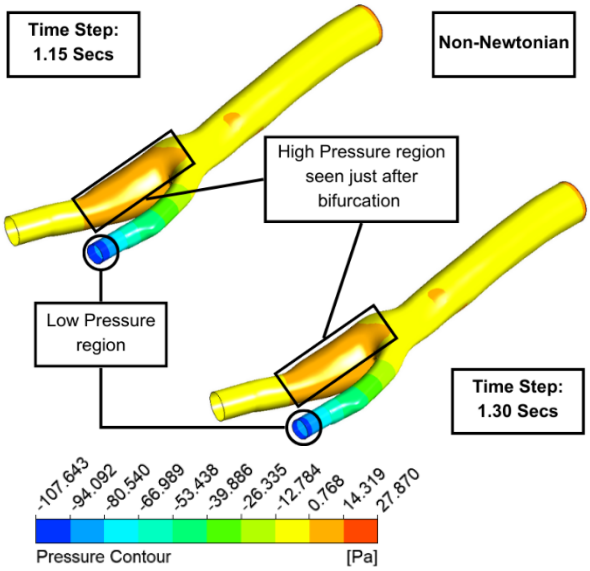

Figure 15. Pressure Contours of Non-Newtonian model.

In this case, the Newt model assumes a constant viscosity, which means that the flow behavior is not affected by the shear rate. Consequently, the pressure distribution remains relatively consistent over a short time interval. Furthermore, the time interval between the two considered time steps in Figure 14 (1.15 seconds and 1.30 seconds) is relatively short. Given the stable flow pattern in the CA, significant changes in the pressure distribution may not occur within such a small time frame. It is important to highlight that although the pressure contours in Figure 14 show minimal variation, it does not imply that the pressure distribution is completely uniform throughout the CA. Localized pressure differences can still exist due to factors such as changes in vessel diameter, variations in wall compliance, and the presence of plaques or stenosis [16].

Figures 15 and 16 represents the pressure contours of the non-newt model, it is evident that the elevated-pressure area is relatively less prominent compared to the Newt model. In the Newt model, the elevated-pressure area ranged between 14.319 and 27.870 Pa, indicating greater magnitudes of pressure. However, in the Non-newt model, the elevated-pressure area appears to be lower, ranging between 0.768 and 14.319 Pa.

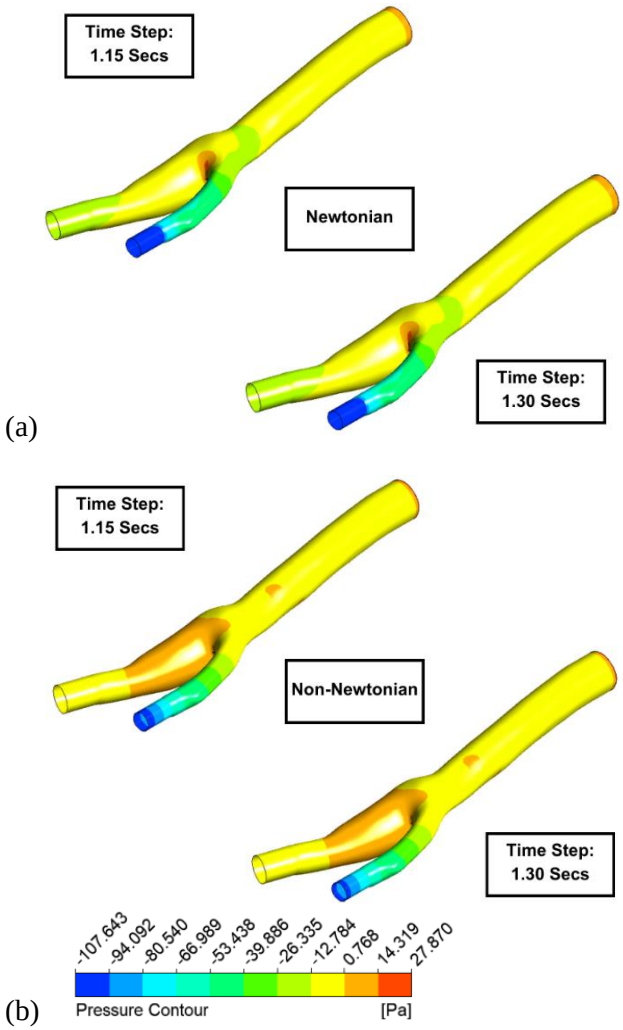

Figure 16. Comparative visuals of both Newtonian (a) and non-Newtonian (b) models.

In this case, the elevated-pressure area appears to occur just after the bifurcations. This suggests that the non-newt viscosity model affects the pressure distribution differently compared to the Newt model. The altered flow behavior in the non-newt model, resulting from reduced resistance to flow due to decreased viscosity under higher shear rates, influences the location and magnitude of the high-pressure region.

These findings emphasize the importance of accounting for blood rheology and considering the specific geometric features of the CA, including the bifurcation, when analyzing the pressure distribution. The Non-newt model provides valuable insights into how the shear-thinning behavior of blood affects the pressure patterns and the potential implications for cardiovascular diseases.

Wall Shear Stress (WSS) Patterns:

The analysis of WSS provides insights into the mechanical stress experienced by the CA walls.

In Figure 17, the WSS contours for the Newt model at both time steps are presented. The regions with low WSS are clearly marked, aligning with the observations from Figures 10 to 12, which indicate low velocity areas. This correlation supports the notion that low WSS is directly linked to regions of reduced velocity within the CA geometry [26]. Additionally, the high WSS regions are also marked in Figure 17, revealing that they predominantly occur in the right bifurcation of the CA. This indicates that the flow dynamics & geometry in the bifurcation region contribute to higher mechanical forces

exerted on the arterial walls, resulting in elevated WSS. The identification of low WSS regions is particularly important as it has been associated with the initiation and development of atherosclerotic plaque formation [25]. These regions, characterized by low mechanical stress on the arterial walls, provide a conducive environment for plaque accumulation. Understanding the spatial distribution of low WSS can aid in identifying areas prone to plaque development and inform targeted interventions to mitigate the risk of cardiovascular diseases. The WSS contours in Figure 17 provide valuable insights into the mechanical forces acting on the CA walls. By considering the specific geometry of the carotid artery, the correlation between low WSS and low velocity, as well as the identification of high WSS regions in the bifurcation, this analysis enhances our understanding of the hemodynamics and potential sites of plaque formation.

Figure 17 represents the counterpart of the Newt model, showcasing the WSS contours for the non-newt model. The analysis reveals that regions with low WSS in the Non-newt model are similar to those in the Newt model. Likewise, the high WSS regions also exhibit similar patterns in both models, primarily observed in the bifurcated right portion of the CA geometry. However, there are notable changes in the magnitude of the WSS values between the two models, particularly in the regions of low WSS. Within the Non-newt model, the wall shear stress (WSS) values span from 0.455 to 0.909 Pa, with certain regions exhibiting WSS close to 0 Pa. Conversely, in the Newt model, the low WSS regions exhibit values close to 0 Pa. Moreover, when examining the regions with high WSS, the Non-newt model shows values ranging from 2.273 to 5 Pa. In contrast, the Newt model primarily exhibits high WSS values between 4.545 and 5 Pa, with only a small portion in the bifurcated right region of the CA displaying WSS values lower than 0.455 Pa.

Figure 18 represents the counterpart of the Newt model, showcasing the WSS contours for the non-newt model. The analysis reveals that regions with low WSS in the Non-newt model are similar to those in the Newt model. Likewise, the high WSS regions also exhibit similar patterns in both models, primarily observed in the bifurcated right portion of the CA geometry. However, there are notable changes in the magnitude of the WSS values between the two models, particularly in the regions of low WSS. Within the Non-newt model, the wall shear stress (WSS) values span from 0.455 to 0.909 Pa, with certain regions exhibiting WSS close to 0 Pa. Conversely, in the Newt model, the low WSS regions exhibit values close to 0 Pa. Moreover, when examining the regions with high WSS, the Non-newt model shows values ranging from 2.273 to 5 Pa. In contrast, the Newt model primarily exhibits high WSS values between 4.545 and 5 Pa, with only a small portion in the bifurcated right region of the CA displaying WSS values lower than 0.455 Pa.

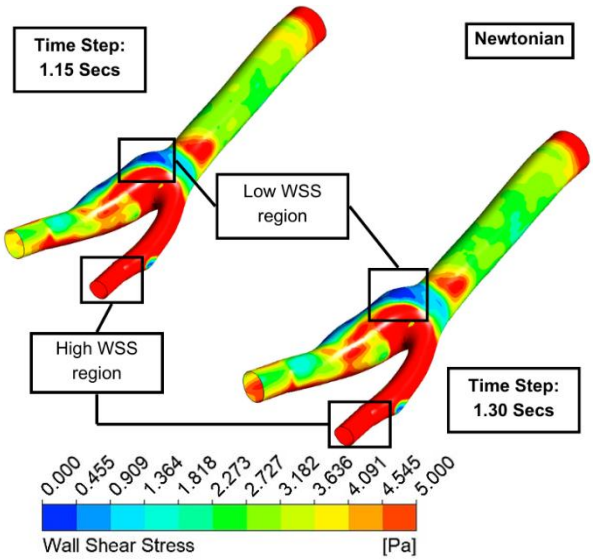

Figure 17. WSS Contour of Newtonian model.

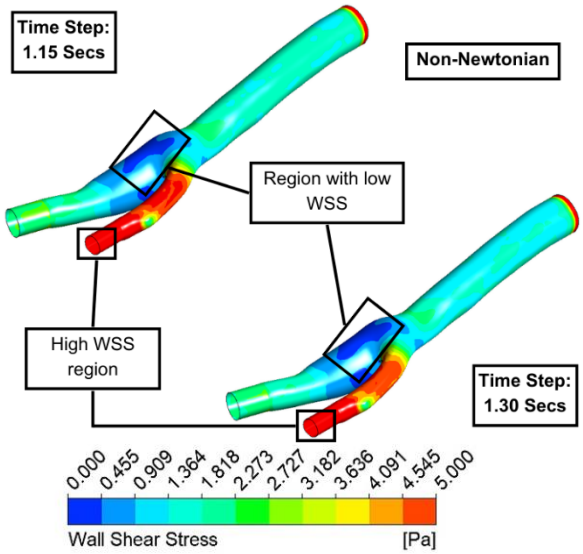

Figure 18. WSS Contour of Non-Newtonian model.

The observed variances in the WSS values between the Non-newt and Newt models can be attributed to the influence of blood rheology and the shear-thinning behavior of blood. In the Non-newt model, the inclusion of a non-newt viscosity model, such as the Carreau model. This means that with the growth of rate of shear, the viscosity of blood declines. Consequently, there is a decrease in resistance to flow, resulting in lower pressure gradients and an altered distribution of wall shear stress (WSS). In regions characterized by low WSS, the Non-newt model exhibits higher WSS values compared to the Newt model. This can be attributed to the decreased viscosity of blood under higher shear rates in the Non-newt model, leading to increased shear stress exerted on the arterial walls. Conversely, in regions with high WSS, the Non-newt model demonstrates lower WSS values compared to the Newt model. This is due to the shear-thinning behavior of blood, where the reduced viscosity under higher shear rates diminishes resistance to flow, subsequently lowering the pressure gradients.

The differences in WSS values between the two models, particularly in regions of low WSS, indicate that the non-newt model allows for a more efficient flow and reduced pressure build-up in the carotid artery. This can have potential implications for minimizing the likelihood of plaque formation. Overall, the incorporation of the non-newt viscosity model captures the shear-thinning behavior of blood and offers a more realistic representation of blood flow in the CA. This variation in the WSS distribution compared to the Newt model and highlights the importance of considering blood rheology in understanding the hemodynamics of the CA. Figure 19 provides comparative visuals of both the models. The comparative analysis between the Non-newt and Newt models in this study provides compelling evidence for the influence of blood rheology on CA hemodynamics.

The observed differences in flow behavior, pressure distribution, and WSS patterns emphasize the critical part of blood rheology in the creation and progression of cardiovascular diseases. The comprehensive insights gained from this study can inform targeted interventions and advancements in cardiovascular medicine. By understanding the impact of blood rheology on CA hemodynamics, researchers and clinicians can devise strategies to optimize patient care outcomes, enhance preventive measures, and develop innovative therapies.

VALIDATION OF STUDY

In order to authenticate the precision and dependability of the simulations performed in this study, an authentication procedure was conducted. The validation intended to compare our results with accessible experimental [27] and numerical data [28], ensuring that our study correctly embodies the real-world behavior of blood flow in the bifurcated CA.

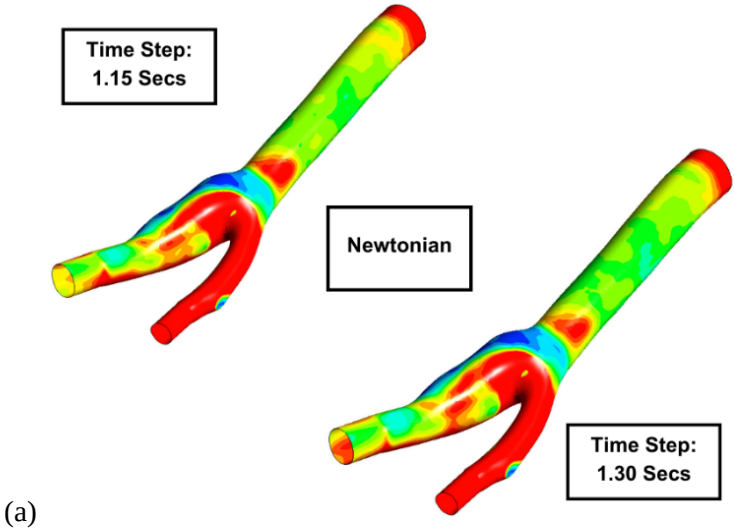

(a)

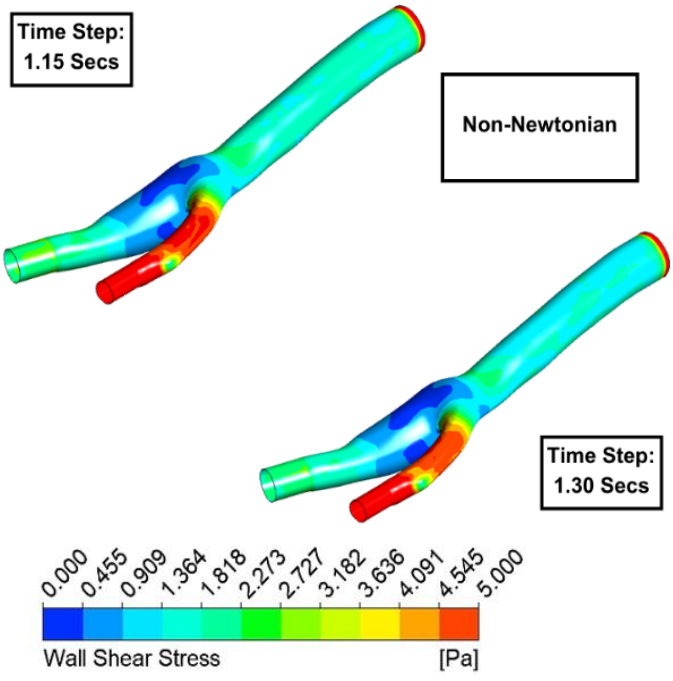

(b)

Figure 19. Comparative visuals of both the models.

Methodology for Comparison

We performed studies for water (Newt fluid) to gauge the accuracy of our study in a bifurcated pipe channel. Later on, we analyzed the results obtained with experimental and numerical datas present in existing literature for the bifurcated channel. The geometry measured for such study entails main artery (height = 30 H, width = H) [27] that breaks into two, approximating a familiar V shape.

3-D Pipe model as seen in Figure 20 was employed to capture simulations for aforementioned scenarios. Figure 21 depicts results of the velocity profiles, are obtained from the current simulations & compared with accessible literature information. The results of the validation course discovered a pleasing level of agreement amid the simulation results and the validation data. It is worth observing that some incongruities were detected in certain sections or under definite stream circumstances. These disparities may be ascribed to the intrinsic complications and boundaries accompanying with both the experimental data and the simulation model. Influences such as measurement errors, assumptions made in the simulation etc., could contribute to these disagreements.

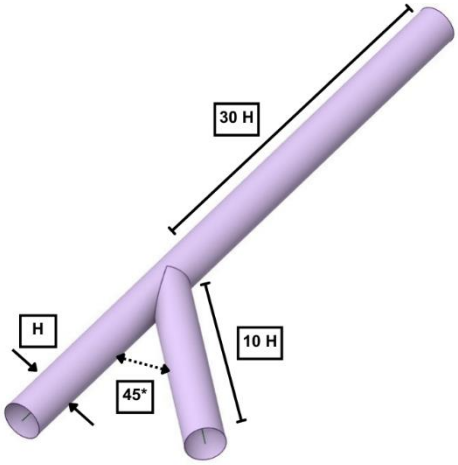

Figure 20. Experimental Pipe Model [27].

Figure 21. Velocity profile of current study with experimental data [27] & computational data [28]

CONCLUSIONS

In this study, we conducted a comparative analysis of blood flow dynamics in the bifurcated CA using Non-newt and Newt models under laminar and pulsatile flow conditions. The results provide valuable insights into the role of blood rheology in CA hemodynamics and its implications for cardiovascular diseases. Through CFD simulations, we observed striking changes amongst Non-newt and Newt models, particularly in regions prone to atherosclerotic plaque formation. The analysis of flow behavior revealed variations in velocity distributions, with the presence of stagnant or recirculating flows, highlighting potential areas of disturbed flow associated with higher plaque deposition risk.

The examination of pressure distribution demonstrated notable differences between the models, particularly in the distal regions of the bifurcation. Variations in mechanical forces acting on the arterial walls were observed, emphasizing the influence of blood rheology on pressure profiles and its potential impact on the development and progression of cardiovascular diseases. The assessment of WSS patterns further revealed substantial disparities between the Non-newt and Newt models. Minimum WSS values indicated areas of low mechanical stress, potentially contributing to endothelial dysfunction and plaque formation. Conversely, regions experiencing high WSS suggested altered hemodynamic conditions. Based on these findings, it is evident that blood rheology plays a critical role in CA hemodynamics. The inclusion of non-newt behavior in the computational models allowed for a more realistic

representation of blood flow, capturing shear-thinning effects and resulting in altered flow patterns, pressure distribution, and WSS patterns.

The implications of this study are significant for understanding and managing cardiovascular diseases. The insights gained from the comparative analysis between Non-newt and Newt models can guide targeted interventions and advancements in cardiovascular medicine. By considering blood rheology, clinicians and researchers can develop improved strategies for risk assessment, prevention, and the development of personalized treatment approaches. It is crucial understand that this study focused on a specific bifurcated CA geometry and utilized computational simulations. Further investigations incorporating patient-specific geometries and experimental validations are necessary to enhance the generalizability and clinical applicability of the findings. Moreover, additional parameters, such as plaque vulnerability indices and flow-induced wall stresses, could be considered in future studies to further explore the complexities of CA hemodynamics.

In conclusion, this comparative analysis of blood flow dynamics in the bifurcated CA highlights the significant differences between Non-newt and Newt models under laminar and pulsatile flow conditions. The findings emphasize the critical role of blood rheology in CA hemodynamics and provide valuable insights into the development and progression of cardiovascular diseases. By understanding and considering the influence of blood rheology, researchers and clinicians can pave the way for advancements in cardiovascular medicine, ultimately leading to improved patient care outcomes.

Acknowledgments

We would like to express our deepest gratitude to our respected and learned guide, Dr. Abdulrajak Buradi, Associate Professor, NMIT, for his invaluable help and guidance throughout this project. We are thankful for his encouragement and support in completing this project. We are also grateful to Dr. Kapilan N, Head of the Department of Mechanical Engineering, NMIT for allowing us to use all the necessary facilities. We also extend our appreciation to the officials and staff members of the Department of Mechanical Engineering at NMIT, who provided us with valuable knowledge and support during our project work. Finally, we would like to express our deep appreciation to our classmates and extend our indebtedness to our parents for their moral support and encouragement.

REFERENCES

1. Mendieta, Jessica Benitez, et al. "The importance of blood rheology in patient-specific computational fluid dynamics simulation of stenotic carotid arteries." Biomechanics and Modeling in Mechanobiology 19 (2020): 1477-1490.
2. Hallad, Nitesh Basavaraj, et al. "Computational Analysis of Blood Flow in a Curved Bifurcated Coronary Artery." Conference on Fluid Mechanics and Fluid Power. Singapore: Springer Nature Singapore, 2021.
3. Mahalingam, Arun, et al. "Numerical analysis of the effect of turbulence transition on the hemodynamic parameters in human coronary arteries." Cardiovascular diagnosis and therapy 6.3 (2016): 208.
4. Kumar, Nitesh, et al. "Effect of Newt and Non-newt flow in subject specific carotid artery." Journal of Engineering Science and Technology 15.4 (2020): 2764-2780.
5. Google Images: https://www.echelon.health/disease_detection/carotid-artery-atheroma/
6. Švancara, Pavel, et al. "Computational Modelling of Blood Flow in the Bifurcation of Human Carotid Artery." 3-Dimensional Modelling in Cardiovascular Disease. Elsevier, 2020. 155-175.
7. Moradicheghamahi, Jafar, Jaber Sadeghiseraji, and Mehdi Jahangiri. "Numerical solution of the Pulsatile, Non-newt and turbulent blood flow in a patient specific elastic carotid artery." International Journal of Mechanical Sciences 150 (2019): 393-403.
8. Buradi, Abdulrajak, and Arun Mahalingam. "Numerical analysis of wall shear stress parameters of Newtonian pulsatile blood flow through coronary artery and correlation to atherosclerosis." Advances in Mechanical Engineering: Select Proceedings of ICRIDME 2018. Springer Singapore, 2020.

9. Google Images: https://www.bupa.co.uk/health-information/heart blood circulation/ischaemic-stroke
10. Hammoud, A., E. Yu Sharay, and A. N. Tikhomirov. "Newt and Non-newt pulsatile flows through CA bifurcation based on CT image geometry." AIP Conference Proceedings. Vol. 2171. No. 1. AIP Publishing LLC, 2019.
11. Buradi, A., and A. Mahalingam. "Effect of stenosis severity on wall shear stress based hemodynamic descriptors using multiphase mixture theory." Journal of Applied Fluid Mechanics 11.6 (2018): 1497-1509.
12. Ahmadpour, Ali, and Arman Khoshnevis. "Numerical Simulation of Non-newt Blood Flow in A Three-Dimensional Non-Planar Bifurcation with Stenosis." Amirkabir Journal of Mechanical Engineering 53.9 (2021): 4865-4886.
13. Hallad, Nitesh Basavaraj, et al. "Computational Analysis of Blood Flow in a Curved Bifurcated Coronary Artery." Conference on Fluid Mechanics and Fluid Power. Singapore: Springer Nature Singapore, 2021.
14. Kumar, Nitesh, et al. "Influence of blood pressure and rheology on oscillatory shear index and wall shear stress in the carotid artery." Journal of the Brazilian Society of Mechanical Sciences and Engineering 44.11 (2022): 510.
15. Buradi, Abdulrajak, Sumant Morab, and Arun Mahalingam. "Effect of stenosis severity on shear-induced diffusion of red blood cells in coronary arteries." Journal of Mechanics in Medicine and Biology 19.05 (2019): 1950034.
16. Rezazadeh, Marzieh, and Ramin Ostadi. "Numerical simulation of the wall shear stress distribution in a CA bifurcation." Journal of Mechanical Science and Technology 36.10 (2022): 5035-5046.
17. Dhungana, Abishek, et al. "Impact of Bifurcation and Bifurcation Angle on the Hemodynamics of Coronary Arteries." Conference on Fluid Mechanics and Fluid Power. Singapore: Springer Nature Singapore, 2021.
18. Pal, Subash Chand, Manish Kumar, and Ram Dayal. "A comparative study of patient-specific bifurcated CA with different viscosity models." Application of Soft Computing Techniques in Mechanical Engineering. CRC Press, 2022. 215-230.
19. Buradi, Abdulrajak, and Arun Mahalingam. "Impact of coronary tortuosity on the artery hemodynamics." Biocybernetics and Biomedical Engineering 40.1 (2020): 126-147.
20. Deshpande, Prahlad V., et al. "Numerical Simulation of Blood Flow Study in an Idealized Bifurcated Coronary Artery." Conference on Fluid Mechanics and Fluid Power. Singapore: Springer Nature Singapore, 2021.
21. Perktold K, Resch M, Florian H. Pulsatile Non-newt blood flow in three-dimensional carotid bifurcation models: a numerical study of flow phenomena under different bifurcation angles. J Biomed Eng. 2022;13(6):507-515.
22. Singh, D., and S. Singh. "A multi-scale computational study of pulsatile flow in the three dimensional human CA bifurcation." Series on Biomechanics (2022).
23. Ramdan, Salman Aslam, et al. "Blood Flow Acoustics in CA." Journal of Advanced Research in Fluid Mechanics and Thermal Sciences 94.1 (2022): 28-44.
24. Nagaharish, G. N., et al. "Blood Flow Analysis Through Bifurcated and Stenosed Coronary Artery." Conference on Fluid Mechanics and Fluid Power. Singapore: Springer Nature Singapore, 2021.
25. Lee S-W, Steinman DA (2007) On the relative importance of rheology for image-based CFD models of the carotid bifurcation. J Biomech Eng 129:273.
26. Dahal, Prabin, et al. "Influence of Blockage on Hemodynamics of Coronary Arteries: A Numerical Investigation." Biennial International Conference on Future Learning Aspects of Mechanical Engineering. Singapore: Springer Nature Singapore, 2022.
27. Liepsch, D., et al. "Measurement and calculations of laminar flow in a ninety degree bifurcation." Journal of biomechanics 15.7 (1982): 473-485.
28. Abugattas, C., et al. "Numerical study of bifurcation blood flows using three different non-Newtonian constitutive models." Applied Mathematical Modelling 88 (2020): 529-549.

